

This discussion paper is/has been under review for the journal Biogeosciences (BG).
Please refer to the corresponding final paper in BG if available.

Calcifying invertebrates succeed in a naturally CO₂ enriched coastal habitat but are threatened by high levels of future acidification

J. Thomsen¹, M. A. Gutowska², J. Saphörster¹, A. Heinemann^{1,3},
K. Trübenbach², J. Fietzke³, C. Hiebenthal⁴, A. Eisenhauer³, A. Körtzinger⁵,
M. Wahl⁴, and F. Melzner¹

¹Biological Oceanography, Leibniz-Institute of Marine Sciences (IFM-GEOMAR), Kiel 24105, Germany

²Institute of Physiology, Christian-Albrechts-University Kiel, Germany

³Marine Geosystems, Leibniz-Institute of Marine Sciences (IFM-GEOMAR), Kiel 24148, Germany

⁴Marine Ecology, Leibniz-Institute of Marine Sciences (IFM-GEOMAR), Kiel 24105, Germany

5119

⁵ Chemical Oceanography, Leibniz-Institute of Marine Sciences (IFM-GEOMAR), Kiel 24105, Germany

Received: 15 June 2010 – Accepted: 22 June 2010 – Published: 2 July 2010

Correspondence to: F. Melzner (fmelzner@ifm-geomar.de)

Published by Copernicus Publications on behalf of the European Geosciences Union.

4000 μatm) in a flow-through seawater system for a period of two weeks (see Table 2 for sea water chemistry) to then obtain haemolymph samples. We found that mussels do not regulate pH_e when exposed to elevated seawater pCO_2 . pH_e followed the non-bicarbonate buffer line when displayed in a Davenport-diagram (Fig. 3, Table 3), suggesting that buffering by extracellular proteins ($1.2 \pm 0.4 \text{ mg mL}^{-1}$, $N=8$ control mussels) is the sole mechanism to stabilize pH_e . The buffer value of the haemolymph is low ($0.49 \text{ mM HCO}_3^- \text{ pH}^{-1}$, Fig. 3), matching findings from other populations of the same species (Booth et al., 1984; Lindinger et al., 1984). Significant reductions in pH_e were found at 142 and 405 Pa (Table 3, Fig. 3a). No significant changes in the concentration of haemolymph Mg^{2+} and Ca^{2+} were observed with respect to treatment pCO_2 (Table 3). While it was proposed that mytilid mussels use HCO_3^- derived from their shells to buffer pH_e (Lindinger et al., 1984; Michaelidis et al., 2005), our results clearly demonstrate that in flow-through seawater experimental designs, *M. edulis* do not maintain extracellular $[\text{HCO}_3^-]$ above that of ambient seawater. This is in contrast to the more active cephalopod molluscs, which greatly elevate extracellular $[\text{HCO}_3^-]$ in order to stabilize pH_e to conserve haemocyanin blood oxygen transport (Gutowska et al., 2010). However, while *M. edulis* does not possess a pH sensitive respiratory pigment, uncompensated pH_e might negatively impact shell formation: comparing control extracellular pH of haemolymph drawn from the posterior adductor muscle with that of the extrapallial fluid (EPF), the fluid that fills the space between mantle and shell surface, indicates that both fluids are characterized by a very similar carbonate system speciation (Table 3B). Assuming that pH_e in the EPF always behaves like that of haemolymph, it is very likely that the inner shell layers (nacre), which primarily consist of aragonite, are in contact with a fluid that is highly under saturated with CaCO_3 : haemolymph $[\text{CO}_3^{2-}]$ is much lower than in seawater $[\text{CO}_3^{2-}]$ at any given seawater pCO_2 (see Fig. 3b). As in addition, only 15% of total EPF $[\text{Ca}^{2+}]$ has been found to be freely dissolved Ca^{2+} (Misogianes and Chasteen, 1979), Ω_{arag} would be even lower at the inner shell interface.

5133

3.3 *M. edulis* growth and calcification (Exp. 2)

To estimate the long-term repercussions of decreased pH_e on the energy budget and the calcification machinery, we conducted a growth trial under optimized feeding conditions (Exp. 2). Previous studies suggested that in mytilid bivalves (*M. galloprovincialis*), uncompensated reductions in pH_e may be causally related to reductions in metabolism (metabolic depression) and somatic growth (Michaelidis et al., 2005). In our 8 week growth study, shell length growth was high under control conditions (3.3 to $4.6 \text{ mm month}^{-1}$ in small vs. medium mussels), fully matching summer field growth rates for mussels of the same size classes in Kiel Fjord (Kossak, 2006). Initial mussel shell length and pCO_2 had significant effects on shell length growth and shell mass increment (see Table 4 for ANOVA results). While shell mass and length growth were similar in control and 142 Pa treated medium sized mussels, both parameters were significantly reduced at 405 Pa (Fig. 4a). In the smaller size group, length growth was significantly reduced at 405 Pa as well. There were no significant differences in shell mass growth in small mussels, although a trend towards lower shell mass was apparent in the 405 Pa group as well (Fig. 4b). However, when displaying shell mass vs. shell length in comparison to wild-type mussels collected from the sampling site in Kiel Fjord (grey symbols in Fig. 4a,b), it appears that all experimental groups lie within the 95% prediction band of the shell mass vs. length function. This indicates that exposure to elevated pCO_2 does not result in the production of a grossly abnormal, thinner shell phenotype; rather, shell growth is slowed proportionally. Regardless of the decreased rates of shell growth at higher pCO_2 (405 Pa), all treatment mussels increased their shell mass at least by 150% during the 8 week trial, even at Ω_{arag} (Ω_{calc}) as low as 0.17 (0.28) (Fig. 4e). This is in contrast to a previous study that has suggested a high sensitivity of mussel calcification to elevated pCO_2 : during acute exposure, a linear correlation between CaCO_3 precipitation rate and seawater pCO_2 (and $[\text{CO}_3^{2-}]$) has been observed in *M. edulis* from the Western Scheldt. A reduction in calcification by about 50% was found at a pCO_2 of ca. 100 Pa (ca. $1000 \mu\text{atm}$), net shell dissolution was ob-

5134

- invertebrates, Mar. Ecol.-Prog. Ser., 373, 275–284, 2008.
- Kurihara, H., Asai, T., Kato, S., and Ishimatsu, A.: Effects of elevated $p\text{CO}_2$ on early development in the mussel *Mytilus galloprovincialis*, Aquat. Biol., 4, 225–233, 2009.
- Lehmann, A., Krauss, W., and Hinrichsen, H. H.: Effects of remote and local atmospheric forcing on circulation and upwelling in the Baltic Sea, Tellus A, 54, 299–316, 2002.
- Lindinger, M. I., Lauren, D. J., and McDonald, D. G.: Acid-base-balance in the sea mussel, *Mytilus edulis*, 3. Effects of environmental hypercapnia on intracellular and extracellular acid-base-balance, Mar. Biol. Lett., 5, 371–381, 1984.
- Mehrbach, C., Culberso, C. H., Hawley, J. E., and Pytkowic, R. M.: Measurement of apparent dissociation-constants of carbonic-acid in seawater at atmospheric-pressure, Limnol. Oceanogr., 18, 897–907, 1973.
- Melzner, F., Gutowska, M. A., Langenbuch, M., Dupont, S., Lucassen, M., Thorndyke, M. C., Bleich, M., and Pörtner, H.-O.: Physiological basis for high CO_2 tolerance in marine ectothermic animals: pre-adaptation through lifestyle and ontogeny?, Biogeosciences, 6, 2313–2331, doi:10.5194/bg-6-2313-2009, 2009.
- Michaelidis, B., Ouzounis, C., Palaras, A., and Pörtner, H. O.: Effects of long-term moderate hypercapnia on acid-base balance and growth rate in marine mussels *Mytilus galloprovincialis*, Mar. Ecol.-Prog. Ser., 293, 109–118, 2005.
- Michaelis, M.: Zur Morphologie und Ökologie von *Polydora ciliata* und *P. ligni* (*Polychaeta, Spionidae*), Helgoländer wiss. Meeresunters., 31, 102–116, 1978.
- Mintrop, L., Perez, F. F., Gonzalez-Davila, M., Santana-Casiano, M. J., and Körtzinger, A.: Alkalinity determination by potentiometry: Intercalibration using three different methods, Cienc. Mar., 26, 23–37, 2000.
- Misogianes, M. J. and Chasteen, N. D.: Chemical and spectral characterization of the extrapallial fluid of *Mytilus edulis*, Anal. Biochem., 100, 324–334, 1979.
- Pörtner, H. O., Langenbuch, M., and Reipschläger, A.: Biological impact of elevated ocean CO_2 concentrations: lessons from animal physiology and earth history, J. Oceanogr., 60, 705–718, 2004.
- Reusch, T. B. H. and Chapman, A. R. O.: Persistence and space occupancy by subtidal blue mussel patches, Ecol. Monogr., 67, 65–87, 1997.
- Ries, J. B., Cohen, A. L., and McCorkle, D. C.: Marine calcifiers exhibit mixed responses to CO_2 -induced ocean acidification, Geology, 37, 1131–1134, 2009.
- Riisgard, H. U., Kittner, C., and Seerup, D. F.: Regulation of opening state and filtration rate in

5141

- filter-feeding bivalves (*Cardium edule*, *Mytilus edulis*, *Mya arenaria*) in response to low algal concentration, J. Exp. Mar. Biol. Ecol., 284, 105–127, 2003.
- Roy, R. N., Roy, L. N., Vogel, K. M., Porter-Moore, C., Pearson, T., Good, C. E., Millero, F. J., and Campbell, D. M.: The dissociation constants of carbonic acid in seawater at salinities 5 to 45 and temperatures 0 to 45 °C, Mar. Chem., 44, 249–267, 1993.
- Thomsen, J. and Melzner, F.: Moderate seawater acidification does not elicit long-term metabolic depression in the blue mussel *Mytilus edulis*, Mar. Biol., submitted, 2010.
- Weiss, R. F.: Carbon dioxide in water and seawater: the solubility of a non-ideal gas, Mar. Chem., 2, 203–215, 1974.
- Yin, Y., Huang, J., Paine, M. L., Reinhold, V. N., and Chasteen, N. D.: Structural characterization of the major extrapallial fluid protein of the mollusc *Mytilus edulis*: implications for functions, Biochemistry, 44, 10720–10731, 2005.

5142

Table 1. Kiel Fjord surface seawater carbonate system speciation 2008 to 2009. Total alkalinity (A_T) and dissolved inorganic carbon (C_T) were measured by potentiometric titration using the VINDTA system and coulometric titration after CO_2 extraction using the SOMMA system. Carbonate system speciation was calculated using the CO2SYS program. See Fig. 1a for corresponding surface pH_{NBS} .

#	Date	S	T (°C)	pH_{NBS}	A_T ($\mu mol\ kg^{-1}$)	C_T ($\mu mol\ kg^{-1}$)	pCO_2 (Pa)	ρCO_2 (μatm)	Ω_{calc}	Ω_{arag}
1	09 Jul 2008	17.4	14.6	7.68	1955.2	1973.1	143	1411	0.79	0.47
2	13 Aug 2008	16.1	18.7	7.83	1913.7	1891.5	104	1026	1.21	0.72
3	08 Sep 2008	19.3	15.5	7.49	2044.9	2106.3	234	2309	0.58	0.35
4	15 Oct 2008	17.3	14.1	7.67	2018.4	2041.3	150	1480	0.79	0.47
5	11 Nov 2008	21.5	11.5	7.86	2063.3	2037.2	91	898	1.22	0.74
6	08 Dec 2008	19.6	7.1	7.98	2123.7	2088.2	68	671	1.34	0.80
7	12 Jan 2009	17.8	3.9	8.01	2078.3	2053.0	62	612	1.18	0.69
8	05 Feb 2009	16.5	3.3	8.10	2113.2	2075.3	52	513	1.36	0.79
9	05 Mar 2009	14.5	3.5	8.23	2067.7	2008.3	39	385	1.67	0.96

5143

Table 2. Seawater carbonate system speciation during experimental trials (mean \pm SD, 14 and 3 determinations for pH , S , T and A_T , C_T). Salinity (S) was 11.8 ± 0.4 and temperature (T) $12.5^\circ C\pm 0.5^\circ C$ in Exp. 1 (duration 2 weeks), $T = 13.8^\circ C\pm 0.6^\circ C$ and $S=15.0\pm 0.6$ in Exp. 2 (duration: 8 weeks).

Treatment	pH_{NBS}	A_T ($\mu mol\ kg^{-1}$)	C_T ($\mu mol\ kg^{-1}$)	pCO_2 (Pa)	ρCO_2 (μatm)	Ω_{calc}	Ω_{arag}
Exp. 1:							
39 Pa/385 μatm	8.05 \pm 0.03	1901.4 \pm 42.2	1841.5 \pm 36.2	47 \pm 2	464 \pm 20	1.77 \pm 0.13	1.01 \pm 0.08
57 Pa/560 μatm	7.89 \pm 0.04	1903.5 \pm 40.8	1873.5 \pm 31.3	67 \pm 5	661 \pm 49	1.31 \pm 0.16	0.75 \pm 0.09
85 Pa/840 μatm	7.81 \pm 0.03	1905.6 \pm 40.3	1891.8 \pm 34.7	80 \pm 3	789 \pm 30	1.09 \pm 0.09	0.62 \pm 0.05
113 Pa/1120 μatm	7.70 \pm 0.03	1906.2 \pm 38.9	1914.3 \pm 34.1	106 \pm 5	1046 \pm 49	0.86 \pm 0.07	0.49 \pm 0.04
142 Pa/1400 μatm	7.56 \pm 0.06	1906.1 \pm 39.3	1943.9 \pm 53.7	150 \pm 31	1480 \pm 306	0.64 \pm 0.09	0.37 \pm 0.05
405 Pa/4000 μatm	7.08 \pm 0.02	1890.8 \pm 25.1	2077.5 \pm 12.0	431 \pm 35	4254 \pm 345	0.22 \pm 0.01	0.12 \pm 0.01
Exp.: 2							
39 Pa/385 μatm	8.13 \pm 0.02	1966.1 \pm 3.2	1891.2 \pm 5.3	50 \pm 3	493 \pm 29	1.94 \pm 0.04	1.14 \pm 0.04
142 Pa/1400 μatm	7.72 \pm 0.06	1968.1 \pm 4.9	1984.4 \pm 12.3	135 \pm 20	1332 \pm 197	0.81 \pm 0.09	0.48 \pm 0.06
405 Pa/4000 μatm	7.26 \pm 0.04	1970.2 \pm 4.3	2125.8 \pm 12.6	395 \pm 22	3898 \pm 217	0.28 \pm 0.02	0.17 \pm 0.01

5144

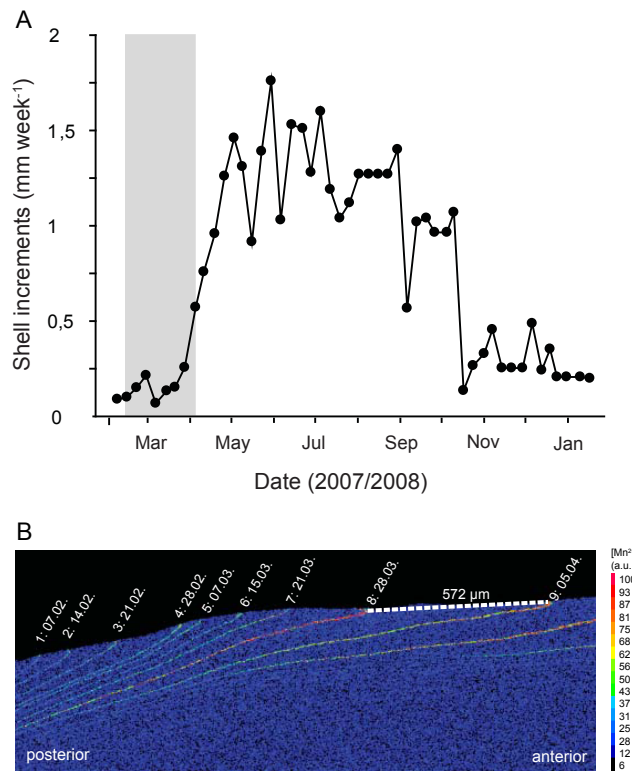


Fig. 2. Manganese marks in the calcite of the shell of a wild *Mytilus edulis* from Kiel Fjord illustrating weekly shell length growth between 07 February 2007 (line 1) and 05 April 2008 (line 9). Shell $[Mn^{2+}]$ in arbitrary units (a.u.). Grey bar in (A) indicates the time interval displayed in (B).

5151

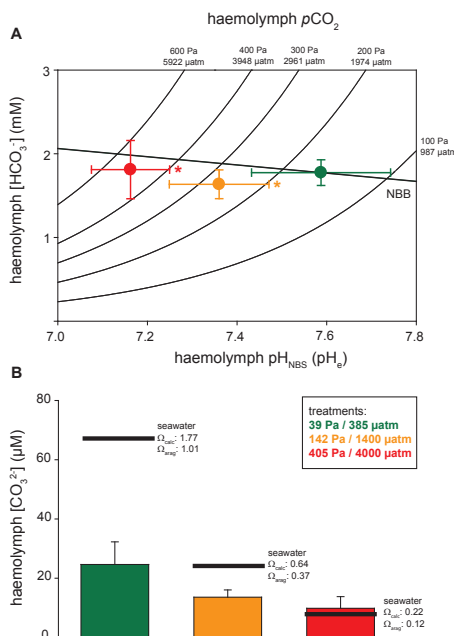


Fig. 3. (Exp. 1): (A) haemolymph acid-base status in relation to environmental pCO_2 (Davenport-diagram) for treatment groups under pCO_2 levels of 39 Pa (ca. 385 μatm , $N=12$), 142 Pa (ca. 1400 μatm , $N=12$) and 405 Pa (ca. 4000 μatm , $N=6$). Isobars represent haemolymph pCO_2 . NBB=non-bicarbonate buffer line. Mussels cannot significantly elevate $[HCO_3^-]$ to compensate pH_e . See also Table 3 and Table 5 for ANOVA tables; (B) (A) Calculated haemolymph $[CO_3^{2-}]$ at seawater pCO_2 values of 39, 142 and 405 Pa (385, 1400, 4000 μatm). Black lines indicate seawater $[CO_3^{2-}]$ and the corresponding $CaCO_3$ saturation state (Table 4 for ANOVA tables).

5152

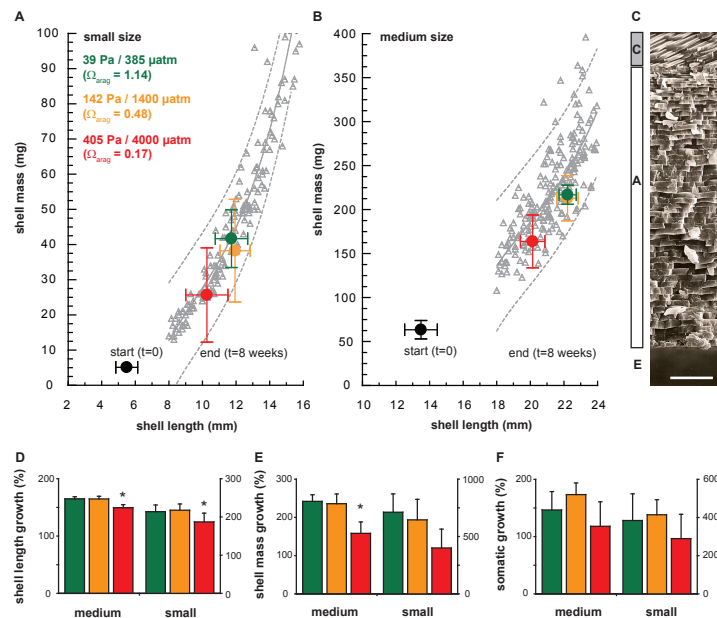


Fig. 4. (Exp. 2): **(A and B)**: Shell mass vs. shell length relationships of small and medium experimental mussels at the beginning of the experiment (black) and after 8 weeks (red, orange, green; means and standard deviation). The grey symbols represent individual mussels from the collection site, the dashed line gives the 95% prediction interval for the shell mass vs. length relationship of wild mussels. **(C)**: SEM cross-section of *M. edulis* shell (detail), showing calcite **(C)** and aragonite **(A)** layers. Aragonite layers are in direct contact with the extrapallial fluid (EPF, E). Scale bar=10 μm. **(D–F)**: Percent shell mass and length, as well as somatic (dry mass) growth over the entire 8 week period. See Table 4 for ANOVA tables.

5153

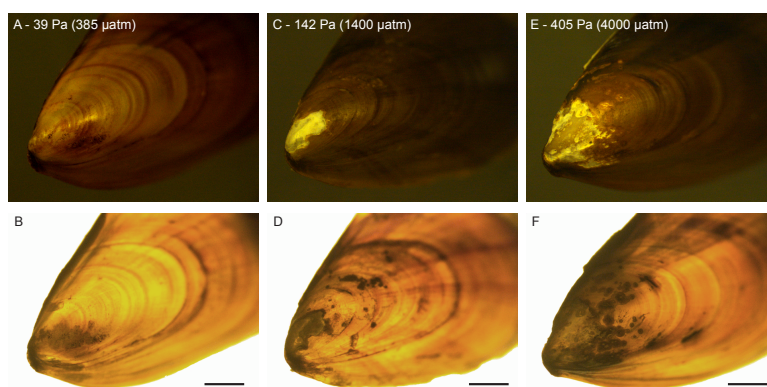


Fig. 5. (Exp. 2): External shell dissolution at the umbo region. Images of umbones of medium sized shells taken under reflected **(A, C, E)** and transmitted **(B, D–F)** illumination to quantify shell dissolution area and severity. In **(E and F)**, dissolution spots are visible as darker regions, as corroded shell material blocks the light stronger than intact crystal structures. **(A and D)** 39 Pa (385 μatm), dissolution index=1, **(B and E)** 142 Pa (1400 μatm), dissolution index=2, **(C and F)** 405 Pa (4000 μatm), dissolution index=3; scale bars=2.5 mm.

5154

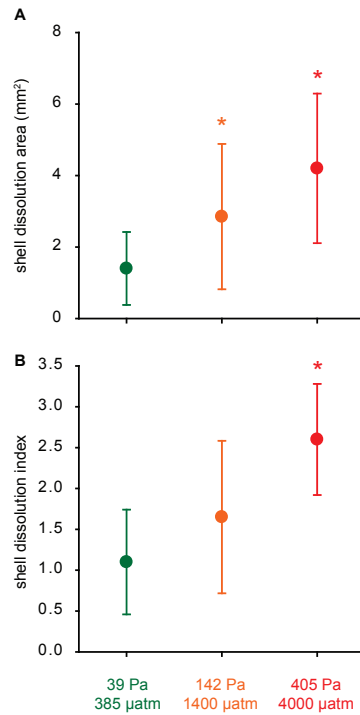


Fig. 6. (Exp. 2): **(A)** shell dissolution area at the umbo region (mm^2) of medium sized mussels, **(B)** shell dissolution index; $N=20$ mussels randomly chosen from the 4 replicate treatments, asterisks indicate significant differences from control (39 Pa, 385 μatm) using Dunn's test. See Table 4 for Kruskal-Wallis test results.

5155

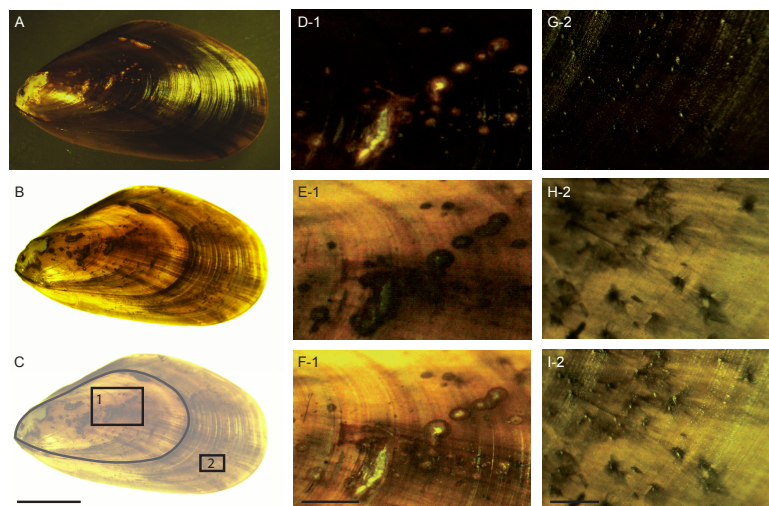


Fig. 7. (Exp. 2): Example of a medium sized mussel (405 Pa, 4000 μatm) with dissolution spots on old and newly formed parts of the shell. **(A–C)** overview, reflected light **(A)**, transmission light **(B)**, position of close-up areas 1 and 2 **(C)** which are depicted in **(D–I)**. Close up area 1 **(D–F)** is located on pre-experimental shell parts (black trace in **(C)** indicates the size of the mussel at the start of the experiment), close-up area 2 **(G–I)** on newly formed shell material. **(D and G)** are reflected light pictures, **(E and H)** are transmission images, **(F and I)** combined reflected and transmission images. White spots are corroded calcite material that is visible when the periostracum is fractured. These spots appear dark when viewed under transmission light. Scale bars: **(A–C)** 5 mm, **(D–F)** 1 mm, **(G–I)** 0.5 mm.

5156